Signal Processing 105 (2014) 122–136

Contents lists available at ScienceDirect

Signal Processing

journal homepage: www.elsevier.com/locate/sigpro

Automatic image segmentation using salient key point extraction and star shape prior

Xiangli Liao [a,b], Hongbo Xu [b], Yicong Zhou [c], Kunqian Li [a], Wenbing Tao [a,e,*], Qiuju Guo [b], Liman Liu [d]

[a] School of Automation and National Key Laboratory of Science & Technology on Multi-spectral Information Processing, Huazhong University of Science and Technology, Wuhan 430074, China
[b] The college of physical science and technology, Central China Normal University, Wuhan 430074, China
[c] Department of Computer and Information Science, University of Macau, Macau, China
[d] School of Biomedical Engineering, South-Central University for Nationalities, Wuhan 430074, China
[e] State Key Laboratory for Novel Software Technology, Nanjing University, Nanjing, China

ARTICLE INFO

Article history:
Received 27 September 2013
Received in revised form
28 March 2014
Accepted 29 April 2014
Available online 9 May 2014

Keywords:
Graph cut
Salient point
Star shape prior
Affinity propagation cluster
Unsupervised image segmentation

ABSTRACT

In this paper, a new unsupervised segmentation method is proposed. The method integrates the star shape prior of the image object with salient point detection algorithm. In the proposed method, the Harris salient point detection is first applied to the color image to obtain the initial salient points. A regional contrast based saliency extraction method is then used to select rough object regions in the image. To restrict the distribution of salient points, an adaptive threshold segmentation is applied to the saliency map to get the saliency mask. And then the salient region points can be obtained by placing the saliency mask on the initial Harris salient points. In order to make sure the salient points which we get are inside the image object thus the star shape constraint can be applied to the graph cuts segmentation, the Affinity Propagation (AP) clustering is employed to find the salient key points among the salient region points. Finally, these salient key points are regarded as foreground seeds and the star shape prior is introduced to graph cuts segmentation framework to extract the foreground object. Extensive experiments and comparisons on public database are provided to demonstrate the good performance of the proposed method.

1. Introduction

Extracting foreground objects of interest from the complex background is of great practical significance in the research of computer vision, pattern recognition and digital image processing. Due to the complexity of modeling a vast amount of visual patterns that appear in generic images and the intrinsic ambiguities in image perception, especially when there is no specific task to guide the attention, image segmentation is found to be difficult and challenging. A general purpose of the image segmentation technique is that it should be able to accurately define the desired object boundaries or regions. In general, existing image segmentation algorithms can be divided into two categories: interactive and automatic methods.

Over the past decades, interactive image segmentation methods have been developed extensively and can be classified into the boundary-based and region-based methods [1]. Boundary-based methods segment the foreground with the boundary information provided by the

* Corresponding author at: School of Automation and National Key Laboratory of Science & Technology on Multi-spectral Information Processing, Huazhong University of Science and Technology, Wuhan 430074, China. Tel.: +86 27 87540164.
E-mail address: wenbingtao@hust.edu.cn (W. Tao).

http://dx.doi.org/10.1016/j.sigpro.2014.04.035
0165-1684/

user. For example, intelligent scissors [2] allow a user to roughly trace the object's boundary with a mouse, and the segmentation result corresponds to the minimum cost path from the cursor position back to the last given point. Active Contours are a class of methods to detect the object by optimizing the initial approximate boundary. The evolution of the given boundary is achieved by optimizing an energy function of image terms and intrinsic regularization terms. Examples include snakes [3], active contours [4], geodesic active contours [5] etc. Region-based methods require users to loosely hint the object and background respectively and then try to maintain a connection of the boundary pixels in progress of segmentation. Magic wand in Photoshop, intelligent paint [6] and marker drawing [7] belong to this category. Boykov and Jolly [8] proposed an effective algorithm for region-based interactive segmentation using graph cuts. Its interactive operations are easy and consist of a few mouse-clicks to indicate some pixels inside or outside the object of interest. A boundary and region information based energy function is then minimized subject to these applied constraints. The global minimum is found by using a graph cut technique. Tao et al. [43] proposed an interactive method based on the variation model and graph cuts to partition the image into multiple scenes. However, those interactive methods use the image information separately in the process of segmentation and often lead to poor segmentation results for objects with weak edges, in clutter, or under occlusion. Thus, accurate segmentation requires more interactions as well as a higher computation cost.

To reduce interactions while obtaining more accurate segmentation results, the shape prior was introduced into the interactive image segmentation. Dambreville [9] integrated the kernel principal component analysis (KPCA) with shape priors in a geometric active contour (GAC) framework. Yeo [10] presented a new variation model for the level-set segmentation using statistical shape priors. A number of algorithms using a parameterized template for the object shape have been proposed for graph cuts segmentation [11,12]. For a specific type of objects, these methods should carry out a mass of statistical learning to obtain the general shape feature information, which increases the computation cost of segmentation. Slabaugh [13] showed how to integrate an elliptical shape prior with the graph cuts segmentation to deal with a certain class of shapes called the elliptical shape. Das [14] presented a similar method to incorporate the shape prior with a graph cuts model for shapes defined as the compact shape. Although these shape prior assumptions are beneficial to segmentation, the explicit representation of an object is restricted by the object shape that limits its application in practice. Veksler [15] investigated a generic shape (called the star shape prior) for the graph cuts segmentation. The prior based on simple geometric properties is much more generic than the previous shape constrains while the star shaped objects are abundant in the nature world. Then [16] extended a single point [15] to multiple points and the Euclidean rays were replaced by geodesic paths.

Though interactive segmentation has been applied to many problems, there are still many drawbacks. Because of a large amount of information in images and their unpredictable complexity, interactive segmentation is tedious, time consuming and impractical, especially when we handle long image sequences. In extremely complex scenes, a great deal of user interactions is needed to obtain a satisfactory result. The main limitations of the above-mentioned segmentation methods are that we have to do interactive operations and cannot achieve automatic segmentation.

Automatic methods can provide segmentation results without any user-interaction. One of main directions of current researches is to define segmentation as an energy function through a graph such as Ncut [17]. Besides graph based methods, there are also other types of image segmentation approaches that mix the features and spatial information together, such as the mean shift [18], watershed algorithm [19] and DDMCMC [20]. However, Ncut [17] based segmentation approaches generally require high computation complexity. It is difficult to segment a natural image into meaningful regions using the mean shift method due to the number and shape of the unknown data cluster. The watershed algorithm [19] often causes a set of over-segmentation problems. The DDMCMC [20] method suffers from the heavy computation burden. Liu and Tao [44] presented an iteratively unsupervised image segmentation algorithm based on the multiphase multiple piecewise constant model and its graph cuts optimization. Four-Color theorem is used to relabel the regions in an image after every iteration process, which makes it possible to represent and segment an arbitrary number of regions in image with only four phases. However, using only color information to describe color-texture objects will generate some small and scatter regions without any visual sense.

The main idea of this paper is to develop an automatic image segmentation method using object star shape prior constraint and salient point detection technology. In [15], the user needs to select a point inside the object as the foreground seed which is the star center at the same time. Given this seed, the system integrates a star shape prior with the graph cuts algorithm to get accurate segmentation of images. Based on [15,16] extends single star center into multiple stars. Consequently, if the star centers can be found automatically, we can easily devise an automatically unsupervised segmentation algorithm. We notice that, in recent years, salient point technique has been widely employed in many applications [21–23] due to its great advantages such as abundant information, simple calculation and a small amount of data. In order to achieve the automatic image segmentation, we use the salient point detection method to try to obtain the star centers of the image objects. What needs to be considered is that these points should be inside the object. However, the existing salient point detection methods have the defect that the detected salient points appear both in the foreground and background. While this is acceptable in some applications, here it is crucial to find the salient points that faithfully exist inside the object, so that the star model method can extract the objects in an image. To achieve this goal, we design a strategy to automatically locate the star centers of the object that has a star shape and ensure they are inside the objects. Firstly, the salient points in the image

are detected by the Harris salient point detection method [29]. Then the salient region detection approach [31] is employed to reduce the distribution of salient points. Secondly, the salient key points are extracted as the star centers. Because a saliency map is the fuzzy region of the object, there may be some salient region points not belonging to the object region. The AP clustering [32] is used to limit the salient key points within the object. Thus the star centers are obtained. Finally, we consider the obtained star centers as the foreground seeds and integrate the star shape prior into the graph cuts algorithm to achieve automatic segmentation.

The block diagram of our proposed unsupervised image segmentation algorithm is given in Fig. 1. Firstly, the Harris salient points are extracted from the original images in (b). At the same time the salient region and its binary result by an adaptive threshold segmentation method are obtained in (c) and (d). Combining the Harris salient points in (b) and the saliency mask in (d) the salient region points are obtained in (e). And then salient key points are extracted by AP clustering in (f). The salient key points are considered as the star centers of the objects and are integrated into graph cuts segmentation framework to get the final segmentation results in (g).

The remainder of the paper is organized as follows. For the explanation of the proposed algorithm, we first briefly review the results of [15,16], as well as the graph cuts model with the star shape constraint in Section 2. An algorithm to select the salient key points automatically is presented in Section 3. Section 4 shows the experimental results of the proposed method. Finally, brief conclusions are drawn in Section 5.

2. Star shape prior for graph cuts

Shape priors have been incorporated into the graph cuts segmentation model in a variety of ways to improve the segmentation performance. However, some of these methods are quite restrictive on the shape of the object, such as the elliptical prior [13] and compact shape prior [14]. Other techniques need to build a shape model firstly through statistical training of segmented objects, and then attempt to find the segmentation that best fits the shape model. These requirements restrict their application [11,12]. However, the star shape we are going to illustrate is very generic and abundant in real nature scenes. In this section we begin with a clear definition of the star shape and then introduce the graph cuts model. Finally, we show how to impose the star-convexity constraint on the segmentation.

The star-convex set is a mathematical concept defined in the geometry and math communities [33,34]. Veksler [15] first used such set as a shape prior and introduced it into the graph cuts segmentation. Now, we give its understandable definition. Intuitively, if one thinks of $\boldsymbol{y}$ as a region surrounded by a wall, $\boldsymbol{y}$ is a star shape if one can find a vantage point c from which any point p in $\boldsymbol{y}$ is within line-of-sight (see Fig. 2(a)). We use 1 and 0 as the object and background labels respectively, and $y_p$is the label of pixel p and y_q is the label of pixel q, where $y_p \in \{0,1\}$ and $y_q \in \{0,1\}$. According to the definition of $\boldsymbol{y}$, the star constraints are written as the following energy function:

$$\forall q \in \Gamma_{c,p}, E^*_{p,q}(y_p, y_q) = \begin{cases} \infty & \text{if } y_p = 1 \text{ and } y_q = 0 \\ 0 & \text{otherwise} \end{cases},$$

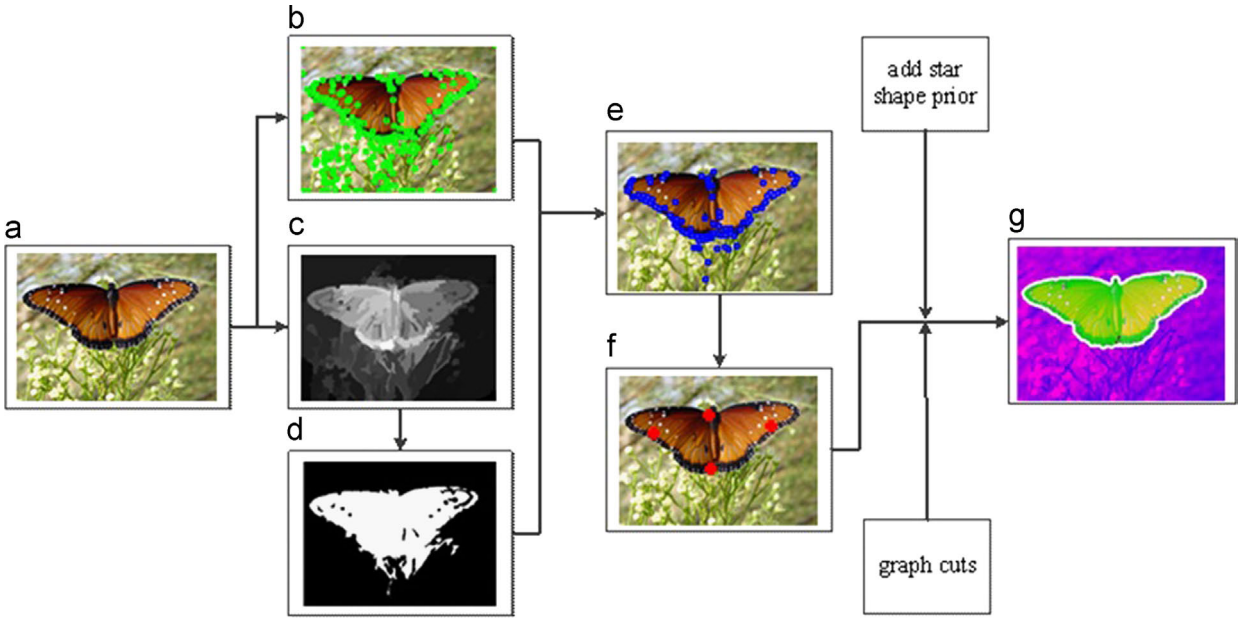

Fig. 1. Block diagram of our automatic image segmentation method. (a) Original image. (b) Harris salient point detection result. (c) Salient region result and (d) is the binary image of (c) by using an adaptive threshold segmentation method. (e) Salient points on the saliency cut map. (f) Salient key points after AP clustering of (e). (g) Final segmentation result using the graph cuts method with the star shape prior provided based on (f).

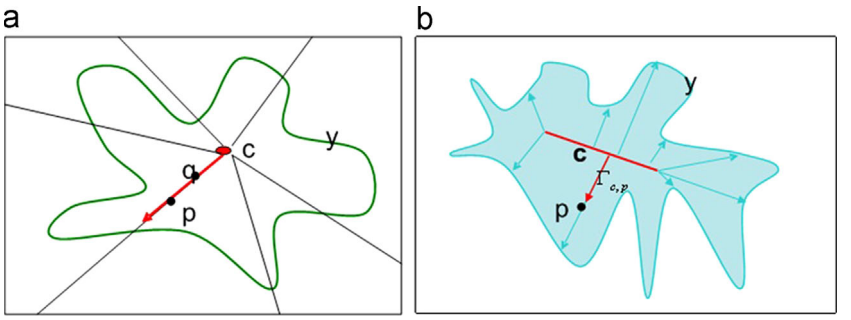

Fig. 2. (a) Object $\boldsymbol{y}$ (in green) in the image domain is a star shape if we can find a center (red dot c) of the object satisfying the condition: to any point p in the object, the point q that lies between c and p is also in the object. In another words, if you are standing at c, you can see all the places in $\boldsymbol{y}$ without occlusion. (b) We treat O as the set of centers. $\forall p \in \mathbf{y}$, it should be visible to its nearest center noted by $c(p)$. (a) Single star and (b) multi star. (For interpretation of the references to color in this figure legend, the reader is referred to the web version of this article.)

$$E^*(\mathbf{y}|c) = \sum_{p \in \Omega} \sum_{q \in \Gamma_{c,p}} E^*_{p,q}(y_p, y_q), \tag{1}$$

where $\Gamma_{c,p}$ is the straight line from c to p. In the practical application, Ω is the discrete image domain. The paths $\Gamma_{c,p}$ are the rasterization of continuous lines. Points p and q correspond to image pixels and (p, q) implies the neighboring pixel pair. In implementation, as [15,16], we also select the point q among 8-connected neighboring pixels (p, q) and calculate the energy directly in the discrete domain.

Gulshan [16] extended a single star to multiple stars for the purpose of expanding the application of the star shape prior (see Fig. 2(b)). The key step is to extend the single center c to an infinite set of centers O, and simultaneously the straight line $\Gamma_{c,p}$ connecting star center c to p is extended to the set of lines $\Gamma_{O,p}$ connecting star centers O to p. Use the mathematical formula for expression:

$$c(p) = \arg\min_{c \in O} d(c, p), \Gamma_{O,p} = \Gamma_{c(p),p}. \tag{2}$$

whertae $d(c,p)$ is the Euclidean distance from c to p, and $c(p)$ is the nearest center to p. The shortest straight line from p to the center set O is denoted by $\Gamma_{O,p}$. According to [16], every point p in $\boldsymbol{y}$ should be visible to its nearest center. Then replace the $\Gamma_{c,p}$ in the energy function in Eq. (1) with $\Gamma_{O,p}$. The expression becomes

$$E^*(\mathbf{y}|O) = \sum_{p \in \Omega} \sum_{q \in \Gamma_{O,p}} E^*_{p,q}(y_p, y_q). \tag{3}$$

The above discussions are based on the Euclidean space. In order to further extend the visibility and reduce the number of center points, [16] proposed the geodesic stars by extending the shortest paths $\Gamma_{O,p}$ from the straight Euclidean rays into geodesic paths. In the discrete domain, the shortest geodesic paths $\Gamma_{O,p}$ are expressed as follows:

$$\Gamma_{O,p} = \arg\min_{\Gamma \in P_{O,p}} L(\Gamma), \tag{4}$$

where $P_{O,p}$ denotes a set of all discrete paths between a set of points c and the point p, $L(\Gamma)$ is the length of a discrete path, the parameter r_g controls the weight between the geodesic and Euclidean for computing the star shape energy. In our experiment, we set r_g=0.3 for all images.

$$L(\Gamma) = \sum_{i=1}^{n-1} \sqrt{(1-r_g) d(\Gamma^i, \Gamma^{i+1})^2 + r_g \|\nabla I(\Gamma^i)\|^2}. \tag{5}$$

To calculate the path, we use the information provided by gradients in the underlying image. In the section, when we define the discrete path, we use $\{\Gamma^1, \Gamma^2, \cdots, \Gamma^n\}$ to denote the n pixels. The notations Γ^i and Γ^{i+1} are used to imply the continuing pixels and $i \in [1, n-1]$. Here n is the number of pixels and Γ is the parametric expression of the discrete path. Here $d(\Gamma^i, \Gamma^{i+1})$ denotes the Euclidean distance between pixels and $\|\nabla I(\Gamma^i)\|^2$ denotes the finite difference approximation of the image gradient between the points (Γ^i, Γ^{i+1}). The parameter r_g controls the weight between the geodesic and Euclidean. Due to the introduction of the underlying image, the star energy $E^*(\mathbf{y}|O)$ is rewritten as $E^*(\mathbf{y}|\mathbf{x}, O)$. The notation $\mathbf{x}$ expresses the image we are processing. We can express the energy as in Eq. (3) with the shortest paths given by Eq. (4). More details can be found in [16].

The graph cuts segmentation model is chosen in this paper as [15,16] do. The energy function used for segmentation in [8] is usually given by

$$E(\mathbf{y}|\mathbf{x}) = \sum_{i \in \Omega} U(y_i|\mathbf{x}) + \lambda \sum_{(i,j) \in N} V(y_i, y_j|\mathbf{x}), \tag{6}$$

where $\mathbf{x}$ is the image, Ω denotes the set of all pixels, N denotes the set of neighboring pixel-pairs and λ is the weight parameter. The data term $U(y_i|\mathbf{x})$ measures the consumption of assigning the label y_i to pixel i, while $V(y_i, y_j|\mathbf{x})$ measures the cost of assigning the labels y_i and y_j to the adjacent pixels i, j.

Then the star shape prior $E^*(\mathbf{y}|\mathbf{x}, O)$ is combined with the graph cuts segmentation. With the constraints, the energy function in Eq. (6) becomes

$$E(\mathbf{y}|\mathbf{x}) = \sum_{i \in \Omega} U(y_i|\mathbf{x}) + \lambda \sum_{(i,j) \in N} V(y_i, y_j|\mathbf{x}) + \gamma E^*(\mathbf{y}|\mathbf{x}, O), \tag{7}$$

$$\mathbf{y} = \arg\min_{\mathbf{y} \in S^*(O)} E(\mathbf{y}|\mathbf{x}), \tag{8}$$

where $S^*(O)$ denotes all the star shapes that put O as the center, the parameter λ is a weight on boundary term $V(y_i, y_j|\mathbf{x})$ in the energy function in Eq. (7), we set λ=150 and γ=10 for all images. The minimum value of the energy

function in Eq. (7) corresponds to the best segmentation. Our goal is to find the star-convex y which satisfies the energy function in Eq. (8). With the shape prior, the segmentation result is more accurate. However, the major limit is that the centers of the object need to be provided by the user. If these points can be found automatically, we can then develop an automatic image segmentation algorithm without user interactions.

3. Automatic salient key points generation

Salient points are commonly employed in a wide variety of applications, including stereo matching, image retrieval and object recognition. Great efforts have been made to investigate salient point detection. There are three main methods to guide the detection process: contour based, parametric model based methods and intensity based [24]. Image contour based methods [25,26] detect the object edge and then calculate salient points using the geometric features along the image edge. The result of this detection algorithm depends heavily on the image contour, which leads to the poor precision. Parametric model methods define salient points based on the image matching degree with the template. For example, Rohr [27] proposed a model associated with the L-corner. Due to the need of template, the application is limited to specific types of salient points. Image intensity based methods detect salient points by directly calculating the pixel values. Moravec [28] developed a salient point detector based on the auto-correlation function. Harris and Stephens [29] improved the Moravec's method by using the auto-correlation matrix. For Smith and Brady (SUSAN detector), salient points are pixels that have few neighbors with similar values [30]. Localization accuracy is one of the most often used criterions to evaluate salient points [24,35]. There are many different salient point detection approaches seeking for locating all salient points as accurate as possible in the image. What special attention should be paid to is that here we are not characterizing the image by the information of salient points purely, but using them as clues to the star shape constraints based on the graph cuts segmentation. Therefore, we must eliminate the unnecessary salient points outside the object for the sake of accurate segmentation.

In this section, we will introduce the salient key point extraction method which integrates the classical Harris salient point detection algorithm, salient region extraction algorithm [31] and AP clustering [32] technologies. With this method, the salient points of an image can be effectively limited inside the object.

3.1. Salient region points

3.1.1. Salient points detector

The salient key point extraction method first applies a salient point detection algorithm on the image. Many different approaches to detecting salient points have been proposed and here we select the Harris salient point detection method. Harris salient point detector [29] and its variations [36,37] are the typical salient point detection techniques currently employed in many computer vision applications [38]. Fig. 3(b) shows examples of salient points detected by Harris.

3.1.2. Saliency map

Visual saliency is the perceptual quality that makes an object outstanding its neighbors and thus captures our attention. More recently, a local contrast based salient region detection method has been proposed in [31]. We choose this salient region detection algorithm in [31] to get the saliency map for that the method is fast and easy to deal with a large number of images. In addition, this algorithm yields the full resolution and uniformly highlighted salient regions, thus we can keep almost all salient points inside the object. On the contrary, if one method produces higher saliency values at object edges instead of generating maps that uniformly cover the whole object, we will miss many significant points in the object. The proposed automatic segmentation method is a little bit similar to the segmentation algorithm in [31]. In [31], they use the saliency map to replace the manually selected rectangular region to locate the object, and then extend the interactive method GrabCut to an automatic method. Our proposed method designs a strategy to automatically locate the star centers of the object that has star shape, considers the obtained star centers as the foreground seeds, and integrates the star shape prior into the graph cuts algorithm to achieve automatic segmentation. Fig. 3 (c) shows one example of saliency map by [31].

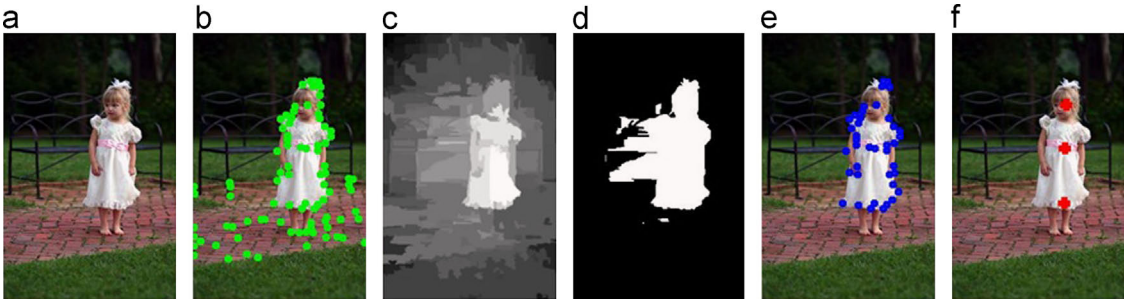

Fig. 3. Given an input image (a). Salient points generated by the Harris detector [29] (b). Salient region result [31] (c) and (d) is the binary image of (c) by using the Otsu threshold method [45]. Salient region points (e). Salient key points (f) produced by the AP clustering which are all in the object.

3.1.3. Saliency mask

After getting the saliency map, a threshold segmentation is applied to the saliency map to get the binary map i.e., the saliency mask. Instead of selecting the threshold empirically [31], we automatically segment the saliency map by using an adaptive threshold segmentation method, i.e., the Otsu method [45], where the segmentation threshold is dynamically determined by maximizing the variance between the target and background. After processing the RC saliency map by the Otsu method, the pixel with a saliency value higher than the threshold is assigned to 1 while the pixel with a lower saliency value is assigned to 0. Therefore, a salient mask is obtained from the RC saliency map. The bright part in the binary image in Fig. 3(d) is the salient mask.

3.1.4. Salient region points

We then place the salient mask on the image with the initial salient points obtained by the Harris salient point detection method [29,36,37] to obtain the salient region points (SRP). Assuming S_P denotes the set of initial salient points and M represents the saliency mask obtained by the Otsu method. Then the salient region points S_{SRP} can be obtained according to the following formula:

$$S_{SRP} = S_P \cap M. \tag{9}$$

The blue points in Fig. 3(e) are the salient region points set S_{SRP}.

3.2. Salient key points by the AP clustering

To exploit the star shape prior in [15,16], we need to constrain the salient points inside the object. Although most of the obtained salient region points above are inside the object which is expected to be segmented out, still some of them are distributed over the background. Notice that the star shape prior method is exactly sensitive to the points outside the object. Our experiments show that the performance of this method in [16] will seriously degenerate when there are a few points which are placed outside the object.

The special process we applied to the image is the AP clustering technology. The AP clustering [32] is based on the affinity propagation and tries to identify each cluster by its exemplar, instead of the virtual geometrical center. The aim of the AP clustering is to find the best set of representative points for the class, maximizing the value of the sum of the similarity between the point and its nearest representative point. And then the exemplars of the salient region points can be used as the centers of the star shape. The main reasons for us to apply the AP clustering algorithm to detect the salient key points lies in three folds: (1) the clustering number need no't be given in prior and the clustering centers will be generated depending on the given points set; (2) the AP clustering algorithm benefits to keep the salient key points inside the object, which is extremely important to the succeeding graph cuts segmentation; and (3) the clustering centers obtained by the AP clustering have good distributions over the object and can effectively represent the object.

The method is carried out based on the similarity matrix formed by the data, and in this paper we choose the Euclidean distance as the test index of the similarity. The AP clustering updates the responsibility and availability of data points by iteration constantly, and the iterative process stops when the iteration times exceed the default threshold or the clustering centers do not change any more. For all images in our experiments, the maximum number of iterations is set as 1000. When we apply the AP clustering to salient region points, the remaining clustering centers are the salient key points. Fig. 3 shows one example how to use the AP clustering to find the salient key points.

4. Experiments comparison and analysis

In this section, we evaluate the performance of our proposed automatic segmentation on a set of images used in [31]. In the graph cuts segmentation framework, the border of the image is fixed to be the background seeds as in [15] and the extracted salient key points are treated as the foreground seeds. Some qualitative analyses of segmentation results will be reported later.

We first introduce a number of parameters that must be appropriately determined for the implementation of the proposed method. Although some of these parameters have been described in the related algorithms, here we still give the settings of all the parameters for the point of clarity and integrity. In Harris salient point detection progress of the Harris salient point detection method, we set the threshold which is used to compute the corner response function given in Eq. (10) as one percent of the maximum value. In the salient region detection process, following the original paper of Cheng [31], we use the region-based contrast (RC) method, as well as its parameters setting. When implementing the AP clustering algorithm, the preference P which controls the number of the clustering center is chosen as min/2 for all images in our experiments, and the maximum number of iterations is set as 1000. We use the parameters setting in [16] for the implementation of the star shape constraint algorithm.

In order to demonstrate the superior performance of our proposed salient key point detection method, other three salient points detection algorithms are chosen in the following experiments for comparison, including the Harris salient point detector [29], SUSAN operator [30] and the Gilles method [39] (see Fig. 4). The results show that the salient points detected by other three classic methods distribute on both the foreground and background regions of the image, and the situation becomes worse when the background is complex (see column 1 of Fig. 4). Comparatively, the proposed salient key point detection algorithm is well suitable for the application cases here. All the extracted salient points are well-distributed inside the objects, which can be regarded as the important object clue of the graph cuts segmentation with the star shape prior.

4.1. The comparison between AP clustering and k-means for salient key points detection

The results in Fig. 5 show the process of our proposed salient key point detection method. Especially, we analyze the superiority of the AP clustering in this algorithm compared with the traditional k-means method.

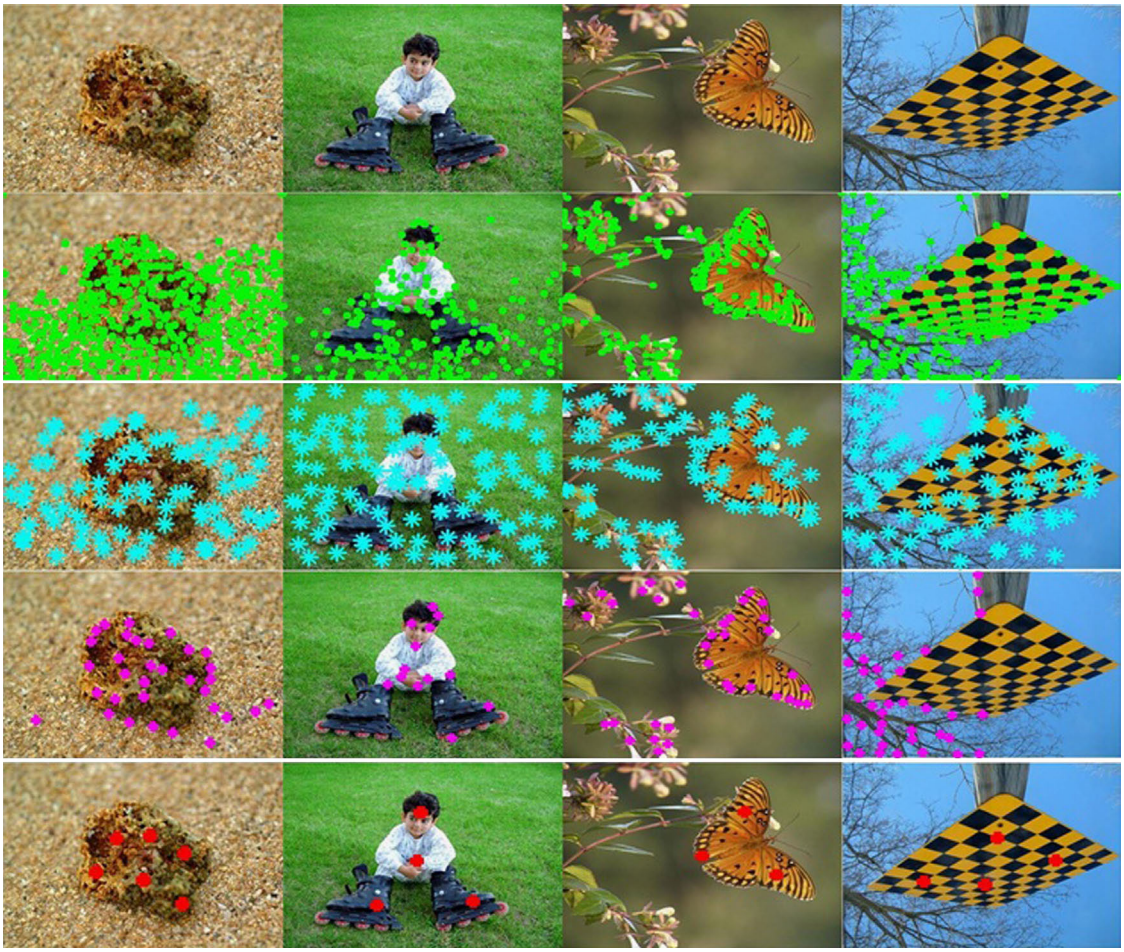

Fig. 4. Visual comparison of salient points. (First row) Original images. (Second row) Harris salient point detection results [29]. (Third row) Salient points produced using [30]. (Fourth row) Salient point detection results of Gilles [39]. (Fifth row) Salient key point detection result by our proposed method.

Given the images in Fig. 5, we first extract the salient points (Fig. 5(a)) using the Harris detector [29], and get the saliency map (Fig. 5(b)) with the method in [31]. The segmentation result of the saliency map by the Otsu algorithm is shown in Fig. 5(c). The salient region points are extracted in Fig. 5(d). From the results, we can see that in the background region most of the salient points in the background are removed and only a small quantity of salient points is left. We further exploit the AP algorithm to cluster the salient region points. The red points in Fig. 5 (e) are the clustering centers obtained by the AP algorithm. We can see that the generated salient key points are all inside the object and can effectively represent the distribution of the object. This is extremely important to the succeeding graph cuts segmentation with the star shape prior. The results in Fig. 5(f) are the segmentation based on the salient key points in Fig. 5(e) by the graph cuts segmentation with the star shape prior. Comparatively, the (g) and (h) in Fig. 5 are respectively the salient key points obtained by the *k*-means and the corresponding segmentation results. From the comparative results we can see that the salient key points obtained by the AP clustering are inside the objects and then their corresponding segmentation results by the graph cuts segmentation with the star shape prior are very good. But not all the salient key points obtained by the *k*-means algorithm are inside the objects and some of them are in the background, so their corresponding segmentation results are worse than the results in Fig. 5(f).

4.2. The comparison with saliency based image segmentation methods

In Fig. 6, the comparative experiments are provided to demonstrate the performance of the proposed automatic image segmentation. In each figure, (a), (b), (c), (d) and (e) are respectively the original test images, the salient point detection results by the Harris algorithm, the salient region points, the salient key points and the segmentation results of our proposed automatic segmentation. The (f) and (g) are the RC-based saliency maps and RC-based saliency cut results (RCC) in [31]. The (h) are the interaction segmentation results of [15] with a user click, and the (i) are the segmentation results of [16] which expanded a single star to multiple geodesic stars with multiple user clicks. The (j) are the Ground truths.

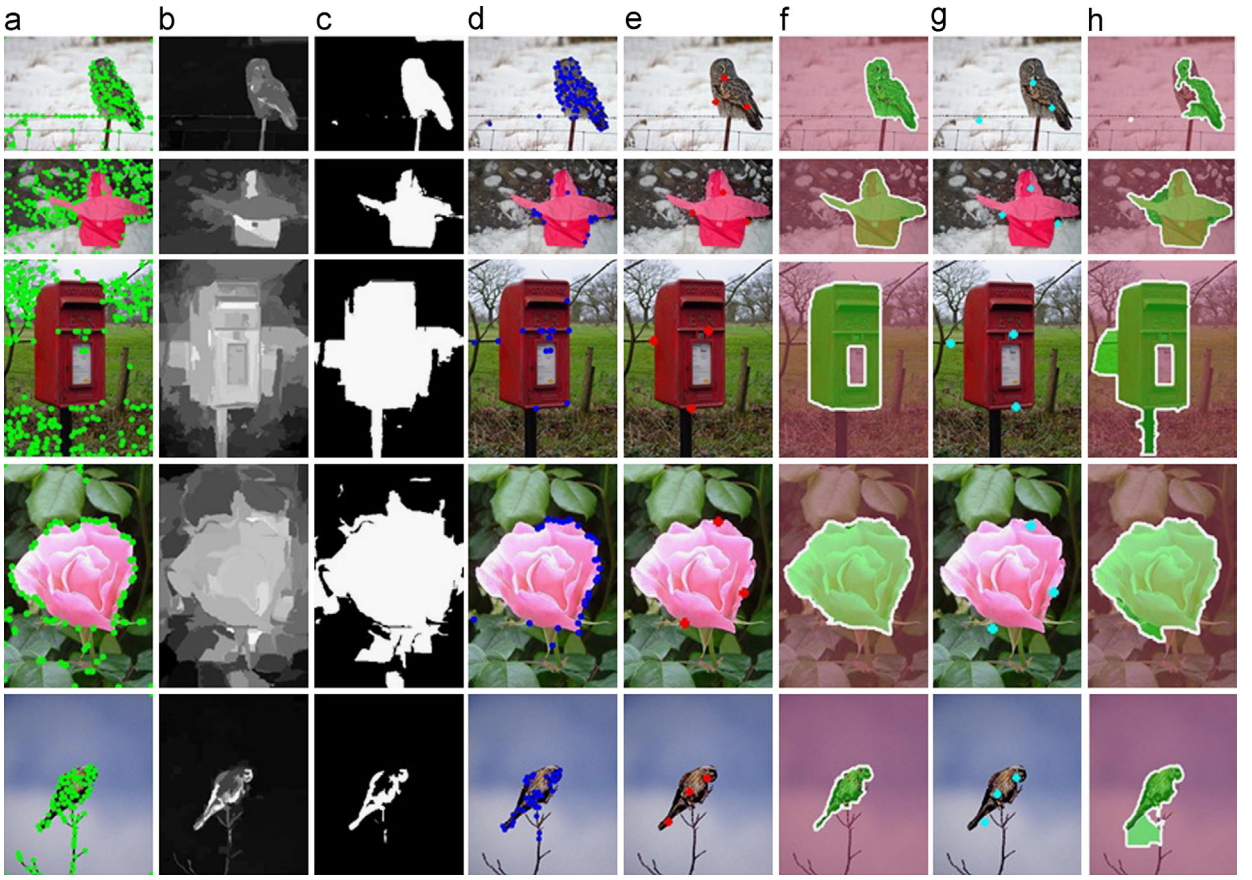

Fig. 5. (a) Original image and salient points. (b) Salient region. (c) Binary image of (b) by using the Otsu method. (d) Salient region points. (e) Salient key points produced by the AP clustering. (f) Segmentation results with star shape constraints based on (e). (g) Salient key points produced by the *k*-means clustering. (h) Segmentation results with star shape constraints based on (g). (For interpretation of the references to color in this legend, the reader is referred to the web version of this article.)

We compare our proposed method with [15] which needs user to select the star center and with [16] which is the improvement of [15]. From the comparison results, we can find that lots of segmentation results of [15] (see Fig. 6 (h)) appear to be seriously under-segmented, and our results are much better than those in [15]. However, although the interactive segmentation method in [16] can choose the user clicks arbitrarily, our proposed automatic method can almost obtain the same good results as in [16] (see the (e) and (i) in Fig. 6). Taking the papaya image in row 11 of Fig. 6 for instance, our proposed method can automatically segment the whole papaya accurately while the method in [15] can just roughly segment the papaya seed region. That is because the method of [15] uses only one user click as the foreground clue, which cannot sufficiently provide the foreground color information, and it can only segment out the middle seed region in the papaya image because the papaya seed region has also satisfied the star shape constraints. Our approach can accurately segment the whole papaya region as [16] does. Considering that the proposed method is an automatic segmentation method, not interactive, the proposed method is more promising in practical application than [16].

Because evaluation methodologies were highly subjective and greatly dependent on intuition, there is not a single correct outcome for an image. To objectively measure the quality of our segmentation results, we have chosen a recently proposed evaluation metric called the probabilistic rand index (PRI) [40,41]. This technique is very generic and is not application specific like some of the earlier ones [42] modeled to account for variability in the human perception. The PRI allows the comparison of a test segmentation result to a set of ground-truth segmentation results through a soft non-uniform weight of pixel pairs as a function of the variability in the ground truth set. For the purpose of better explaining the experiment results, we also show the quantitative comparisons of the global consistency error (GCE) [43] and the variation of information (VOI) [44]. GCE measures the extent to which one segmentation can be viewed as a refinement of other segmentations that are related and in this manner are considered to be consistent, since they could represent the same natural image segmented at different scales. VOI defines the distance between two segmentations as the average conditional entropy of one segmentation result given the other, and thus roughly measures the amount of randomness in one segmentation result.

In order to better demonstrate the superiority of our method, we give the quantitative comparisons of the

Fig. 6. Comparisons of the segmentation results. (a) Original test images. (b) Salient point detection results by the Harris algorithm. (c) Salient region points. (d) Salient key points. (e) Segmentation results of our proposed automatic segmentation. (f) Rc-based saliency maps [31]. (g) RC-based saliency cut results (RCC) [31]. (h) Interaction segmentation results of [15] with a user click. (i) Segmentation results of [16] which expanded a single star to geodesic stars. (j) Ground truths.

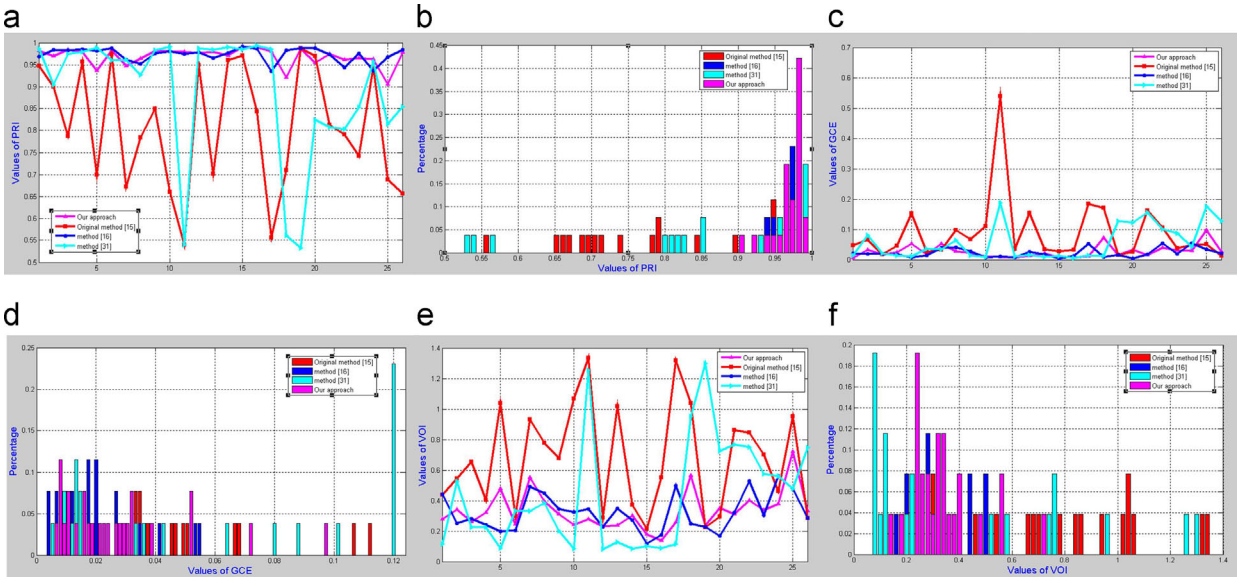

Fig. 7. Quantitative comparisons of the PRI, GCE and VOI for our approach and the original interactive segmentation method [15,16], and the automatic segmentation method RCC [31]. The tested images are provided from Figs. 1–6. (a) PRI, (b) GCE and (c) VOI are values of four methods. The distributions of PRI, GCE and VOI are shown in (d), (e) and (f) respectively.

PRI, GCE and VOI for our approach and three compared methods including the RCC method in [31] and the interactive segmentation method in [15,16]. Corresponding to the segmentation results in Figs. 1–6, the quantitative comparisons of the PRI, GCE and VOI for three compared approaches are displayed in Fig. 7. From the curves in Fig. 7, for most of images in Figs. 1–6, we can observe that the average PRI values of our approach are higher than those of methods in [15,31] and slightly lower than those of the method in [16]. And the GCE values of our approach are almost all lower than those of methods in [15,31], and slightly higher than those of the method in [16]. The VOI values of our approach are lower than those of the method [15], and slightly higher than those of the method in [16]. Though some of the VOI values of our approach are higher than those of the method [31], to analyze the VOI distribution in Fig. 7(f), we can observe that the VOI values of our approach mainly distribute on the lower value area. Since the method [16] is an interactive method where the salient key points are selected by users, it is not surprising that the method [16] has the best performance. The distributions of the PRI, GCE and VOI in Fig. 7(d), (e) and (f), respectively, show that our approach has a bigger percentage in the location with the large PRI, low GCE and VOI values. In addition, for the purpose of further demonstrating the superior performance of our approach, we also show the average values of the PRI, GCE and VOI in Table 1. For instance, the mean (PRI, GCE, and VOI) values of our approach are (0.9685, 0.0269, 0.3344), and those of methods in [15,16,31] are (0.8097, 0.0887, 0.6774), (0.9732, 0.0220, 0.3207) and (0.8895, 0.0581, 0.4322) respectively. These statistics indicate that, in the experiments used in this paper, our approach can acquire the higher accuracy than the compared methods in [15,31] and is a little worse than [16].

We do exhaustive experiments to evaluate the proposed method on several benchmark datasets. MSRA-1000 dataset [53] and MSRA-5000 dataset [54] are commonly used in saliency detection methods. THUS-10000 is the dataset used in [31]. Imgsal-50 is a subset of the Imgsal dataset [56] and comprises 50 images with large salient objects for evaluation. We also test the proposed method on PASCAL VOC2012 dataset [55], which contains complicated images with multiple objects. These datasets contain human-labeled foreground mask as ground truth for segmentation evaluation.

Table 1
Average values of the PRI, GCE and VOI achieved on images in Figs. 1–6.

Methods	Ours	[15]	[16]	[31]
PRI	0.9685	0.8097	0.9732	0.8895
GCE	0.0269	0.0887	0.0220	0.0581
VOI	0.3344	0.6774	0.3207	0.4322

For a given segmentation result, we adopt two criteria to evaluate the quantitative performance of different approaches: at first step, we compute the intersection-over-union score (VOC score) which is standard in PASCAL VOC challenges as follows:

$$R = \frac{R_{fgd} \cap GT_{fgd}}{R_{fgd} \cup GT_{fgd}}, \tag{10}$$

where R_{fgd} and GT_{fgd} are the areas of segmented foreground and the marked ground truth, respectively.

In the second step, we compute the F-measures as

$$F_\beta = \frac{(1+\beta^2)\text{Precision} \times \text{Recall}}{\beta^2\ \text{Precision} + \text{Recall}}, \tag{11}$$

where we set $\beta^2 = 0.3$ as in [31].

The comparison results between the proposed algorithm and RCC [31] on different datasets are shown in Fig. 8. From the results we can see that for the several

datasets the proposed algorithm is better than RCC [31]. We also do quantitative experiments on the 1500 images dataset provided by [59]. We compare our results with the results by [31,53,59] with three criteria, precision, recall rate and *F*-measure. The quantitative comparison of the results is shown in Fig. 9. *F*-measure is computed as Eq. (11) and we also set $\beta^2=0.3$ as in [59]. From the results, we can see that the performances by the proposed method, RCC [31] and GGSIM [59] are close while better than FT [53] and GSIM [59].

4.3. The comparison with different saliency detection algorithms

Our proposed segmentation algorithm is based on the extracted salient key points. Therefore, the saliency detection step has important influence on the final segmentation result. We choose the saliency detection algorithm in [31] for its good performance and competitive computational efficiency. In Figs. 10 and 11, we conduct the comparison experiments to test the segmentation performance of the proposed algorithm framework when different saliency detections are used. Six saliency detection algorithms, the algorithm by Jiang et al. [50], the algorithm by Zhang and Sclaroff [49], the algorithm by Li et al. [51], the algorithm by Yang et al. [48], the algorithm by Yan et al. [46], the algorithm by Siva et al. [47], the algorithm by Cheng et al. [57] and the algorithm Jiang et al. [58] are chosen to compare with Cheng et al. [31]. From the final segmentation results in Fig. 10 we can see that almost all the saliency detection algorithms can get the same segmentations. Since [31] is fast and easy to deal with a large number of images, we adopted [31] as the salient region detection method in our proposed algorithm framework. The statistical comparisons of different salient region detection algorithms in the proposed framework on the MSRA-1000 dataset [53] are shown in Fig. 11. We do an exhaustive comparison with the state-of-the-art saliency methods by two evaluation criterions: VOC score and *F*-measure. Result shows that the results are slightly different when different salient region detection methods are used.

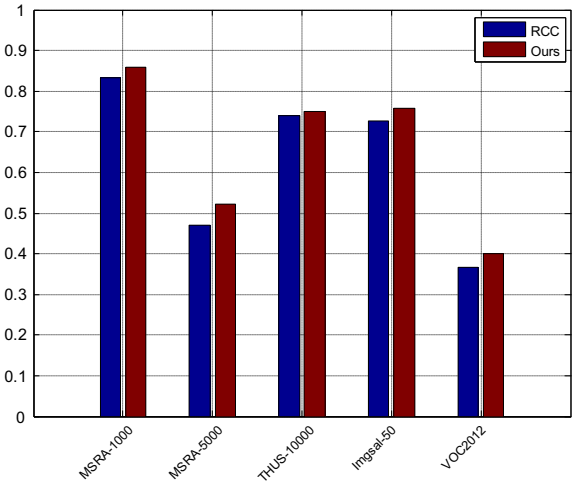

Fig. 8. Statistical comparisons between the RCC [31] method and our proposed method on the datasets MSRA-1000 [53], MSRA-5000 [54], THUS-10000 [31], Imgsal-50 [56] and VOC2012 [55]. We adopted the VOC score to evaluate the performance of the two methods.

4.4. The comparison with different automatic segmentation algorithms

In Figs. 12, 13 and 14, we compare the proposed segmentation method with the other automatic segmentation methods such as the Ncut method [17] and the diffusion segmentation method [52] in terms of the segmentation performance and computational efficiency. Some results are illustrated in Fig. 12, where the clustering number is set $K=4$ in the Ncut method [17] for best performance and the clustering number is set $K=2$ in the diffusion segmentation [52] for best performance. The comparison results in Fig. 12 show that the proposed segmentation method performs best. The statistical comparisons of the average VOC score among the proposed method, RCC [31], Ncut [17] and the Diffusion

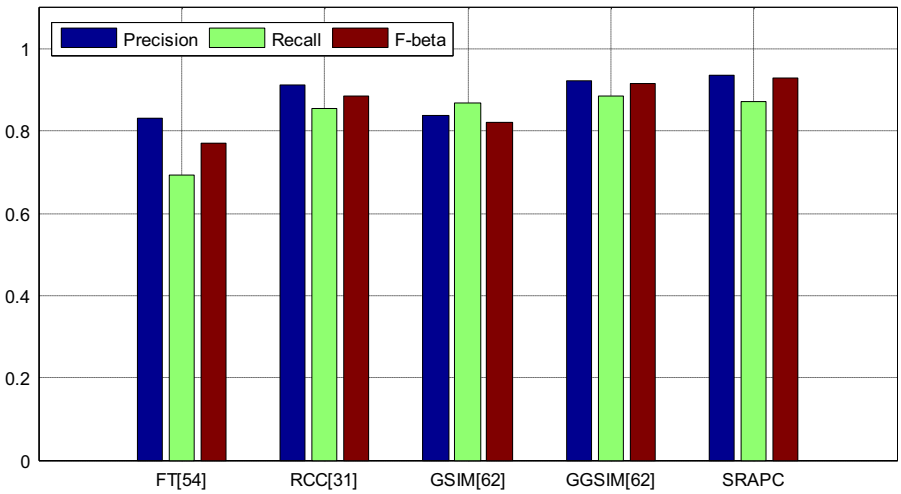

Fig. 9. Precision-recall bars for the results of [31,53,59] and the proposed method over the 1500 images dataset [59].

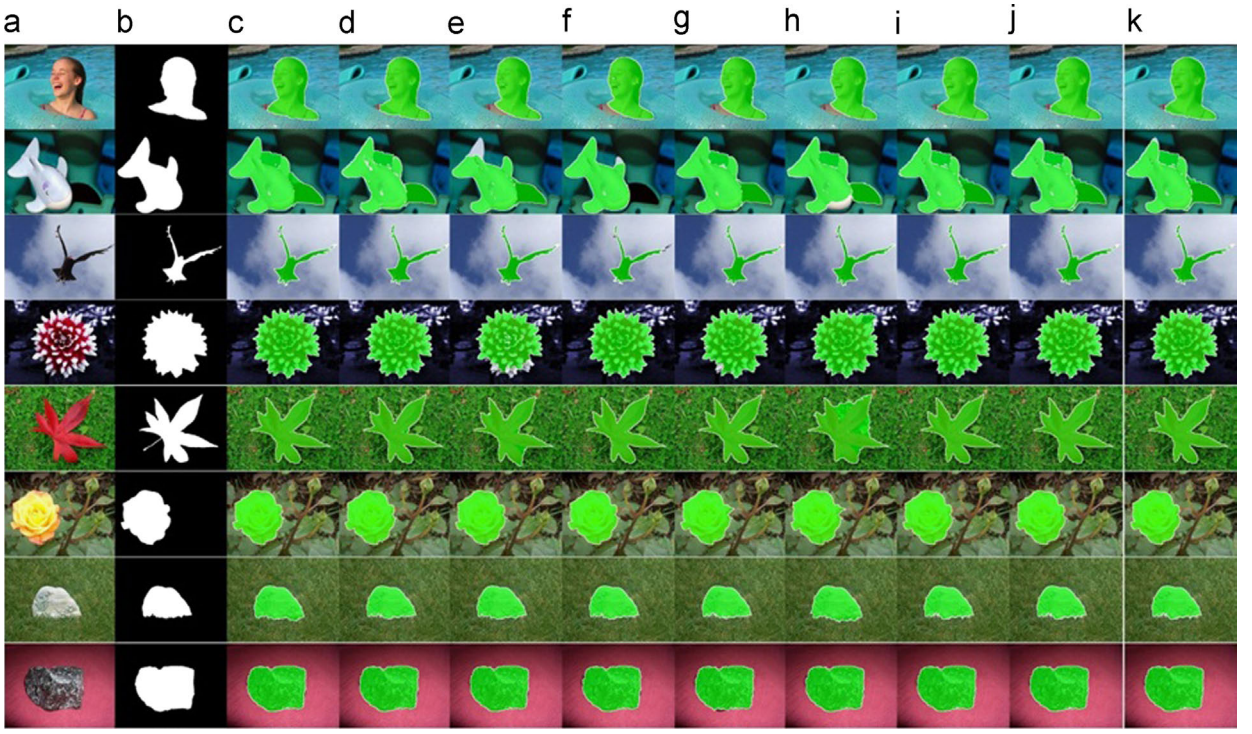

Fig. 10. Comparisons with some latest open source salient region detection methods. (a) Original images. (b) Ground truth. From (c)–(i) is SRAPC using (c) Jiang et al. [50], (d) Zhang and Sclaroff [49], (e) Li et al. [51], (f) Yang et al. [48], (g) Yan et al. [46], (h) Siva et al. [47], (i) Cheng et al. [57], (j) Jiang et al. [58] and (k) Cheng et al. [31].

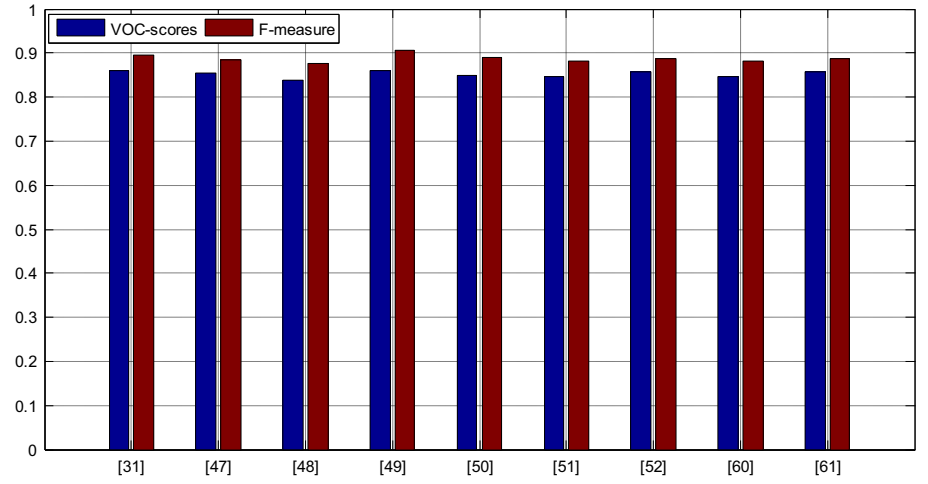

Fig. 11. Statistical comparisons of different salient region detection methods' performance in the proposed method on the MSRA-1000 dataset [53]. We do an exhaustive comparison with state of the art saliency methods by two evaluation criterions: VOC score and *F*-measure. Result shows that our method is slightly different when the salient region detection method changes.

segmentation method [52] on MSRA-1000 dataset are shown in Fig. 13, which demonstrate the superior performance of the proposed algorithm to the three compared algorithms in [17,31,52]. The average time cost comparison among the proposed methods, RCC [31], Ncut [17] and the diffusion segmentation method [52] on MSRA-1000 dataset is shown in Fig. 14. The result shows that the proposed algorithm is slightly slower than RCC [31] while faster than Ncut [17] and the diffusion segmentation [52].

4.5. Experiment on multiple-object image

We also provide the visual experiments on more challenging cases with images selected from PASCAL VOC2012 dataset

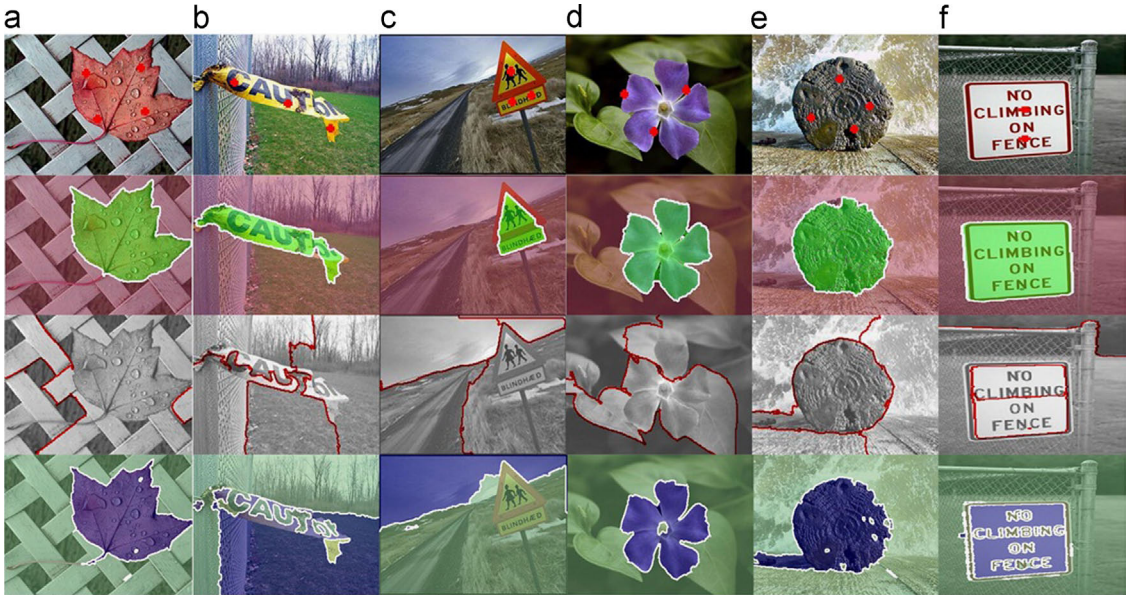

Fig. 12. Comparisons by the proposed method with the Ncut in [17] and the Diffusion segmentation method in [52]. (a) Original test images with the salient key points (star centers). (b) Segmentation results of the proposed automatic segmentation. (c) Partitioning results by directly applying the Ncut method with $K=4$. (d) Segmentation results by [52] with $K=2$.

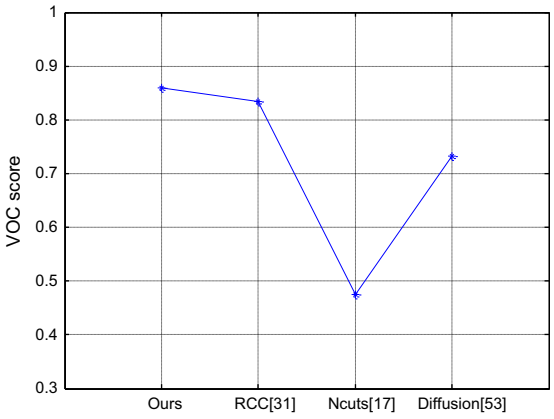

Fig. 13. The performance comparison by the average VOC score for the proposed method, RCC [31], Ncut [17] and the Diffusion segmentation method [52] on MSRA-1000 dataset.

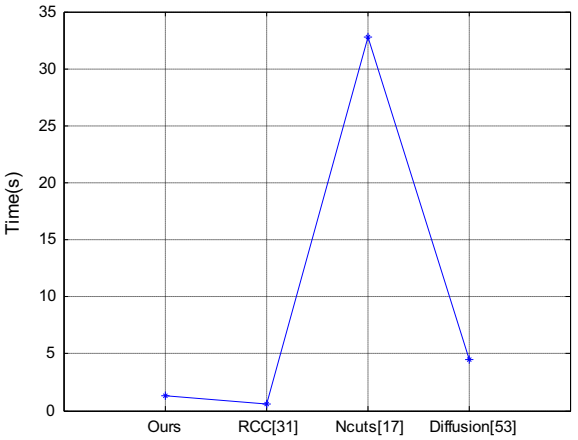

Fig. 14. The average time cost comparison for the proposed method, RCC [31], Ncut [17] and the Diffusion segmentation method [52] on MSRA-1000 dataset.

[55] and the iCoseg dataset [60]. As can be seen, our approach (shown in Fig. 15) can deal well with the challenging cases which are complicated images and multiple-objects images. From the results we can see that the proposed method can effectively extract the salient foreground objects from the images. However, as the proposed method segments each image into only two phases, the foreground and the background just like [31,59] do, although the algorithm can extract all the salient foreground objects, multiple different objects in image are hard distinguished with each other. We also compare the proposed method with the automatic segmentation algorithms [17,52] on the images in Fig. 15. The comparison results show that the proposed method preforms better than [17,52]. We do more quantitative experiments as shown in Fig. 8 in the PASCAL VOC2012 dataset [55], which contains a large number of multiple-object images. The results show that the proposed algorithm is better than RCC [31].

5. Conclusion and discussion

In this paper, we present an automatic image segmentation method integrating salient points with the star shape constraint based on the graph cuts framework. We constructed an automatic object star center extraction method by combining the salient region extraction with the AP clustering technology. Then the obtained star centers are regarded as the foreground seeds and the star shape prior is integrated into the graph cuts algorithm to achieve automatic segmentation. The experiment evaluation and comparison

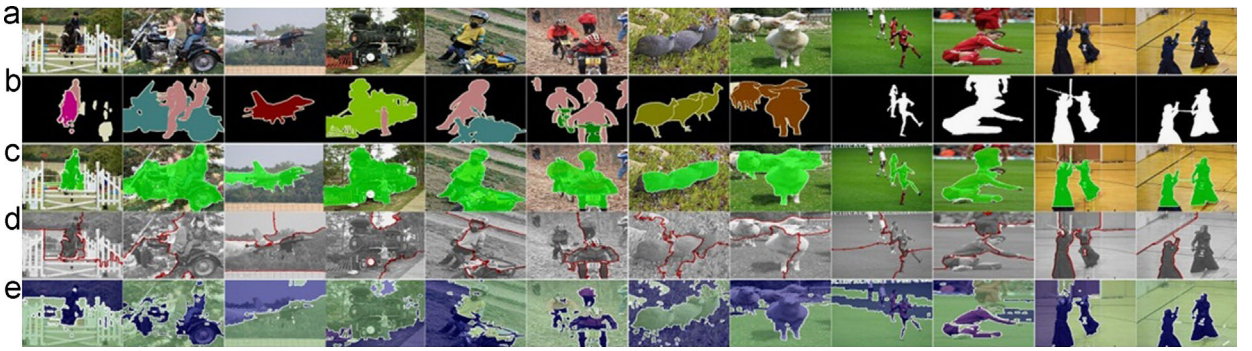

Fig. 15. Some examples from VOC dataset [55] (8 images on the left) and iCoseg [60] (4 images on the right) which include multiple objects. (a) Original images, (b) Ground truth, (c) Segment results with the proposed method, (d) Segment results with Ncut ($K=4$) [17] and (e) Segment results by [52] with $K=2$.

with the other state-of-the-art algorithms on several publicly available datasets has emphasized the good performance of the proposed algorithm.

The proposed method is based on the salient points or region detection. And then the salient key points are extracted for star shape prior. Lastly the graph cuts algorithm based on star shape prior constraint is used to get the final segmentation. Hereby, the proposed method is limited by the extracted salient key points. If the extracted salient key points can cover only one object then the algorithm can segment out one object. While if the salient key points can cover two or multiple objects the algorithm can segment out two or multiple objects. However, most of the existing saliency detection algorithms are concentrated on single object. Therefore, the proposed algorithm has the limitation to deal with multi-object segmentation. The saliency detection for multiple objects is an interesting and challenging topic. We will conduct some research and hope to get some results in the near future.

Acknowledgments

The research has been supported by the National Natural Science Foundation of China, People's Republic of China (61371140, 61273279, and 61305044), Grants 20130144120004, and by the Macau Science and Technology Development Fund under Grant 017/2012/A1, and by the Research Committee at University of Macau under Grants MRG001/ZYC/2013/FST and MYRG113(Y1-L3)-FST12-ZYC.

References

[1] Y., Li, J., Sun, C.K., Tang, H.Y., Shum, Lazy snapping, In: Proceedings of the SIGGRAPH Conference, 2004, pp. 303–308.
[2] E.N. Mortensen, W.A. Barrett, Interactive segmentation with intelligent scissors, Graph. Models Image Process. 60 (5) (1998) 349–384.
[3] M. Kass, A. Witkin, D. Terzopoulos, Snakes: active contour models, Int. J. Comput. Vis. 1 (4) (1988) 321–331.
[4] M. Isard, A. Blake, Active Contours, Springer, New York, 1998.
[5] V. Caselles, R. Kimmel, G. Sapiro, Geodesic active contours, Int. J. Comput. Vis. 22 (1) (1997) 61–79.
[6] L.J. Reese, W.A. Barrett, Image editing with intelligent paint, in: Proceedings of Eurographics, vol. 21(3), 2002.
[7] A.X. Falcao, R. Lotufo, G. Araujo, The image foresting transformation, Relatorio Tecnico IC-00-12, 2000.
[8] Y. Boykov, M.P. Jolly, Interactive graph cuts for optimal boundary and region segmentation of objects in N–D images, in: Proceedings of the International Conference on Computer Vision, 2001, pp. 105–112.
[9] S. Dambreville, Y. Rathi, A. Tannenbaum, Shape-based approach to robust image segmentation using kernel PCA, in: Proceedings of the International Conference on Computer Vision and Pattern Recognition, 2006, pp. 977–984.
[10] S.Y. Yeo, X. Xie, I. Sazonov, P. Nithiarasu, Level set segmentation with robust image gradient energy and statistical shape prior, in: Proceedings of the International Conference on Image Processing, 2011.
[11] D. Freedman, T. Zhang, Interactive graph cut based segmentation with shape priors, in: Proceedings of the International Conference Computer Vision and Pattern Recognition, 2005, pp.755–762.
[12] J. Malcolm, Y. Rathi, A. Tannenbaum, Graph cut segmentation with nonlinear shape priors, in: Proceedings of the International Conference on Image Processing, vol. 4, 2007, pp. 365–368.
[13] G. Slabaugh, G. Unal, Graph cuts segmentation using an elliptical shape prior, in: Proceedings of the International Conference on Image Processing, vol. 2, 2005.
[14] P. Das, O. Veskler, V. Zavadsky, Y. Boykov, Semi-automatic segmentation with compact shape prior, in: Proceedings of the International Conference on Image and Vision Computing, vol. 27, 2009, pp. 206–219.
[15] O. Veksler, 2008. Star shape prior for graph-cut image segmentation, in: Proceedings of ECCV.
[16] V. Gulshan, C. Rother, A. Criminisi, A. Blake, A. Zisserman, Geodesic star convexity for interactive image segmentation, in: Proceedings of CVPR.
[17] J. Shi, J. Malik, Normalized cuts and image segmentation, IEEE Trans. Pattern Anal. Mach. Intell. 22 (8) (2000) 888–905.
[18] D. Comaniciu, P. Meer, Mean shift: a robust approach toward feature space analysis, IEEE Trans. Pattern Anal. Mach. Intell. 24 (5) (2002) 603–619.
[19] L. Vincent, P. Soille, Watersheds in digital spaces: an efficient algorithm based on immersion simulation, IEEE Trans. Pattern Anal. Mach. Intell. 13 (6) (1991) 583–597.
[20] Z. Tu, S.-C. Zhu, Image segmentation by data-driven markov chain monte carlo, IEEE Trans. Pattern Anal. Mach. Intell. 24 (5) (2002) 657–673.
[21] R. Rahmani, S.A. Goldman, H. Zhang, S.R. Cholleti, J.E. Fritts, Localized Content-Based Image Retrieval, IEEE Trans. Pattern Anal. Mach. Intell. 30 (11) (2008) 1902–1912.
[22] C. Wolf, J.M. Jolion, W. Kropatsch, H. Bischof, Content based image retrieval using interest points and texture features, in: Proceedings of the International Conference on Pattern Recognition (ICPR'00), vol. 4, 2000, p. 4234.
[23] C. Lee, J. Leou, H. Hsiao, Saliency-directed color image segmentation using modified particle swarm optimization, Signal Process. 92 (1) (2012) 1–18.
[24] C. Schmid, R. MOHR, C. Bauckhage, Evaluation of interest point detectors, Int. J. Comput. Vis. 37 (2) (2000) 151–172.
[25] E. Shilat, M. Werman, Y. Gdalyahu, . Ridge's corner detection and correspondence, in: Proceedings of the Conference on Computer Vision and Pattern Recognition, Puerto Rico, USA, 1997, pp. 976–981.

[26] F. Mokhtarian, A. Mackworth, Scale-based description and recognition of planar curves and two-dimensional shapes, IEEE Trans. Pattern Anal. Mach. Intell. 8 (1) (1986) 34–43.
[27] K. Rohr, Recognizing corners by fitting parametric models, Int. J. Comput. Vis. 9 (3) (1992) 213–230.
[28] H.P. Moravec, Towards automatic visual obstacle avoidance, in: Proceedings of the 5th International Joint Conference on Artificial Intelligence, Cambridge, Massachusetts, USA, 1977, p. 584.
[29] C. Harris, M. Stephens, A combined corner and edge detector, in: Proceedings of the Fourth Alvey Vision Conference, 1988, pp.147–151.
[30] S.M. Smith, J.M. Brady, SUSAN – a new approach to low level image processing, Int. J. Comput. Vis. 23 (1) (1997) 45–78.
[31] M.M. Cheng, G.X. Zhang, N.J. Mitra, X. Huang, S.M. Hu, Global contrast based salient region detection, in: Proceedings of the IEEE Computer Society Conference on Computer Vision and Pattern Recognition (CVPR), 2011.
[32] B.J. Frey, D. Dueck, Clustering by passing messages between data points, Science 315 (5814) (2007) 972–976.
[33] De Xu Songhe Feng, X.u. Yang, Attention-driven salient edges and regions extraction with application to CBIR, Signal Process. 90 (1) (2010) 1–15.
[34] C.R. Smith, A characterization of star-shaped sets, Am. Math. Monthly 75 (4) (1968) 386.
[35] N. Sebe, M.S. Lew, Comparing salient point detectors, Pattern Recognit. Lett. 24 (2003) 89–96.
[36] K. Mikolajczyk, C. Schmid, Scale & affine invariant interest point detectors, Int. J. Comput. Vis. 60 (1) (2004) 63–86.
[37] I. Laptev, On space–time interest points, Int. J. Comput. Vis. 64 (2) (2005) 107–123.
[38] L. Matthies, M. Maimone, A. Johnson, Y. Cheng, R. Willson, C. Villalpando, S. Goldberg, A. Huertas, A. Stein, A. Angelova, Computer vision on mars, Int. J. Comput. Vis. 75 (1) (2007) 67–92.
[39] S. Gilles, Robust Description and Matching of Images (Ph.D. thesis), University of Oxford, Oxford of Britain, 1998.
[40] R. Unnikrishnan, M. Hebert, Measures of similarity, in: Proceedings of the Seventh IEEE Workshop on Computer Vision Applications, 2005, pp. 394–400.
[41] R. Unnikrishnan, C. Pantofaru, M. Hebert, Toward objective evaluation of image segmentation algorithms, IEEE Trans. Pattern Anal. Mach. Intell. 29 (6) (2007) 929–944.
[42] J.S. Cardoso, L. Corte-Real, Toward a generic evaluation of image segmentation, IEEE Trans. Image Process. 14 (11) (2005) 1773–1782.
[43] Wenbing Tao, Feng Chang, Liman Liu, H. Jin, T. Wang, Interactively multiphase image segmentation based on variational formulation and graph cuts, Pattern Recognit. 43 (2010) 3208–3218.
[44] Liman Liu, Wenbing Tao, Image segmentation by iterative optimization of multiphase multiple piecewise constant model and Four-Color relabeling, Pattern Recognit. 44 (2011) 2819–2833.
[45] N. Otsu, A threshold selection method from gray-level histograms[J], IEEE Trans. Syst. Man Cybern. 9 (1) (1979) 62–66.
[46] Q. Yan, L. Xu, J. Shi, J. Jia, Hierarchical saliency detection, in: Proceedings of CVPR, 2013.
[47] P. Siva, C. Russell, T. Xiang, L. Agapito, Looking beyond the image: unsupervised learning for object saliency and detection, in: Proceedings of CVPR, 2013.
[48] C. Yang, L. Zhang, H. Lu, X. Ruan, M.-H. Yang, Saliency detection via graph-based manifold ranking, in: Proceedings of CVPR, 2013.
[49] J. Zhang, S. Sclaroff, Saliency detection: a boolean map approach, in: Proceedings of ICCV, 2013.
[50] B. Jiang, L. Zhang, H. Lu, M. Yang, C. Yang, Saliency detection via absorb Markov chain, in: Proceedings of ICCV, 2013.
[51] X. Li, H. Lu, L. Zhang, X. Ruan, M. Yang, Saliency detection via dense and sparse reconstruction, in: Proceedings of ICCV, 2013.
[52] G. Kim, E.P. Xing, L. Fei-Fei, T. Kanade, Distributed cosegmentation via submodular optimization on anisotropic diffusion, in: Proceedings of ICCV, 2011.
[53] R. Achanta, S. Hemami, F. Estrada, and S. Susstrunk, Frequency-tuned salient region detection, in: Proceedings of CVPR, 2009.
[54] T. Liu, J. Sun, N. Zheng, X. Tang, H.-Y. Shum, Learning to detect a salient object, in: Proceedings of CVPR, 2007.
[55] M. Everingham, L. Van～Gool, C.K.I. Williams, J. Winn, A. Zisserman, The PASCAL Visual Object Classes Challenge 2012 (VOC2012) Results.
[56] J. Li, M. Levine, X. An, X. Xu, H. He, Visual saliency based on scale-space analysis in the frequency domain, IEEE Trans. Pattern Anal. Mach. Intell. 35 (2013) 996–1010.
[57] M. Cheng, J. Warrell, W. Lin, S. Zheng, V. Vineet, N. Crook, Efficient salient region detection with soft image abstraction, in: Proceedings of ICCV, 2013.
[58] H. Jiang, J. Wang, Z. Yuan, Y. Wu, N. Zheng, S. Li, Salient object detection: a discriminative regional feature integration approach, in: Proceedings of CVPR, 2013.
[59] W. Luo, H. Li, G. Liu, K.N. Ngan, Global salient information maximization for saliency detection, Signal Process.: Image Commun. 27 (3) (2012) 238–248.
[60] D. Batra, A. Kowdle, D. Parikh, J. Luo, T. Chen, iCoseg: interactive co-segmentation with intelligent scribble guidance, in: Proceedings of CVPR, 2010.